Journal of Alloys and Compounds 509 (2011) 9708–9717

Contents lists available at ScienceDirect

Journal of Alloys and Compounds

journal homepage: www.elsevier.com/locate/jallcom

Co_2MnO_4 spinel-palladium co-infiltrated $La_{0.7}Ca_{0.3}Cr_{0.5}Mn_{0.5}O_{3-\delta}$ cathodes for intermediate temperature solid oxide fuel cells

Hong Quan He [a], Lan Zhang [b], Alireza Babaei [b], Xin Wang [a], San Ping Jiang [c,*]

[a] School of Chemical and Biomedical Engineering, Nanyang Technological University, 62 Nanyang Avenue, Singapore 639798, Singapore
[b] Energy Research Institute @ NTU, Nanyang Technological University, 50 Nanyang Drive, Singapore 637553, Singapore
[c] Fuels and Energy Technology Institute and Department of Chemical Engineering, Curtin University, Perth, WA 6102, Australia

ARTICLE INFO

Article history:
Received 21 June 2011
Received in revised form 20 July 2011
Accepted 22 July 2011
Available online 3 August 2011

Keywords:
Solid oxide fuel cell
Spinel oxide
Nanostructured electrode
Palladium oxide nanoparticles
Thermal stability
Co-impregnation

ABSTRACT

The effect of co-infiltration of Co_2MnO_4 (CM) spinel oxides and Pd on the electrochemical activity and microstructure stability of $La_{0.7}Ca_{0.3}Cr_{0.5}Mn_{0.5}O_{3-\delta}$ (LCCM) cathodes for the O_2 reduction reaction of intermediate temperature solid oxide fuel cells (IT-SOFCs) has been investigated in detail. The microstructure, thermal stability, electrochemical activity and stability of the Co_2MnO_4–Pd/PdO powders and Co_2MnO_4–Pd/PdO co-impregnated LCCM cathode were measured using thermal gravimetric analysis, X-ray diffraction, scanning electron microscopy and electrochemical impedance spectroscopy. The results indicate that the addition of spinel oxides effectively inhibits the growth and coalescence of the Pd/PdO nanoparticles and stabilizes the microstructure of the Pd/PdO at high temperatures. The best electrochemical activity and stability of LCCM cathodes were obtained on the cathode co-infiltrated with 50 wt% PdO/50 wt% Co_2MnO_4. The enhancement is due to the significantly improved stability of the microstructure as a result of the inhibited grain growth and agglomeration of Pd/PdO nanoparticles by the co-infiltrated Co_2MnO_4 spinel phase.

1. Introduction

In recent years, intermediate temperature solid oxide fuel cells (IT-SOFCs) with operating temperature in the range of 600–850 °C as a clean power source have attracted worldwide attention due to their much higher conversion efficiencies as compared to the conventional energy conversion systems [1,2]; and their distinguished advantages over other types of fuel cells such as system compactness, promising benefits of the increased long-term stability, wide range of material selection and possibility of using low cost interconnect materials and processing techniques [3–12]. Cathode is one of the key components of IT-SOFCs and is the place where pure oxygen or oxygen from air is reduced to oxygen ions through the combination of electrons supplied externally from the cell. Thus, the materials used as the IT-SOFC cathode should have high electronic conductivity and oxygen ionic conductivity, and should also meet the requirement of chemical and thermal stability in an oxidizing environment, chemical and thermal compatibility with the electrolyte, and high catalytic activity toward O_2 reduction reactions at intermediate temperatures [13].

The most common cathode material for the high temperature operation is the lanthanum strontium manganite (LSM) perovskite oxides [14]. LSM has excellent electronic conductivity, good electrocatalytic activity and stability for the oxygen reduction reactions between 900 and 1000 °C [15–18]. However, the electrochemical performance of the LSM cathodes decreases dramatically with the reduced temperature due to the negligible oxygen ion conductivity of LSM [19,20]. LSM-based perovskite oxides also react with Y_2O_3–ZrO_2 (YSZ), forming lanthanum zirconate resistive phase at temperatures higher than 1200 °C [21,22]. This would limit the potential application of the LSM-based materials for the cathode-supported SOFCs prepared by cost effective fabrication techniques. It has been shown that by doping chromium on the B-site of LSM, the stability of LSM can be substantially enhanced. Tao and Irvine reported that there was no secondary phase detected from the mixed $La_{0.75}Sr_{0.25}Cr_{0.5}Mn_{0.5}O_3$ (LSCM) and YSZ powders sintered at 1300 °C for 80 h [23]. LSCM is an interesting material for the potential electrode application in SOFCs, and its crystal structure is stable under both fuel reduction and oxygen oxidation conditions [23,24]. LSCM also shows a higher oxygen ion conductivity as compared to LSM [25]. In our previous studies, LSCM or LSCM-based composite electrodes have shown considerable electrocatalytic activity toward the oxygen reduction reaction as SOFC cathode [26–28].

We have also shown that the proper doping can improve the electrical conductivity and electrochemical activities of lanthanum

* Corresponding author.
E-mail addresses: WangXin@ntu.edu.sg (X. Wang), s.jiang@curtin.edu.au (S.P. Jiang).

0925-8388/$ – see front matter © 2011 Elsevier B.V. All rights reserved.
doi:10.1016/j.jallcom.2011.07.097

chromites based electrode materials [28–30]. For example, replacing strontium with calcium at the A-site of LSCM improves the electrochemical activities for the O_2 reduction reaction. The electrical conductivity of $La_{0.7}Ca_{0.3}Cr_{0.5}Mn_{0.5}O_{3-\delta}$ (LCCM) at 800 °C is 29.9 S cm^{-1} and the electrode polarization (interfacial) resistance (R_E) on LCCM/YSZ composite cathodes is 0.5 Ω cm^2 at 900 °C [28]. The results show that LCCM is a good candidate for the cathodes of IT-SOFCs.

Solution infiltration is very attractive in the development of nano-structured electrodes that combine the catalytic and electrochemical active phase with the structural rigidity of porous scaffold for IT-SOFCs [31–34]. It has been shown that the electrocatalytic activity of cathodes for IT-SOFCs can be significantly improved by infiltrating wide range of catalytic active nanoparticles, such as GDC [35,36], $La_{0.6}Sr_{0.4}CoO_3$ [37,38], Pd [39,40], $(Ba,Sr)(Co,Fe)O_{3-\delta}$ [41], $Sm_{0.6}Sr_{0.4}CoO_3$ [42], and $Y_{0.5}Bi_{1.5}O_3$ [43]. The enhancement in the electrochemical performance of infiltrated electrodes is truly remarkable. For example, the electrode polarization resistance of the Pd-impregnated YSZ cathodes can be as low as 0.22 Ω cm^2 at 700 °C [44]. However, the most significant challenge in the application of nano-structured electrodes is the long-term stability of the microstructure and performance of the infiltrated nanoparticles. As the particle size of the infiltrated phase is very fine (20–100 nm), the tendency for sintering and grain growth at operation temperature of SOFCs (500–800 °C) is high due to the large surface energy associated with the nano-sized oxide or metallic phase. The grain growth and agglomeration of the impregnated metal catalyst nanoparticles are believed to be the main reason for the observed degradation in the performance stability of the electrodes containing metal catalyst [45]. In the case of infiltrated Pd nanoparticles on porous YSZ scaffold, the agglomeration and grain growth would result in the formation of continuous and dense Pd films on the YSZ scaffold surface, leading to the increase in the polarization losses due to the blocking of the oxygen diffusion path [46]. Alloying with cobalt, manganese and silver has been found to be effective to increase the thermal stability and to enhance the performance stability of Pd-infiltrated electrodes [46,47]. Co-infiltration of mixed ceria and cobalt solutions was also found to suppress the aggregation of Co_3O_4 nanoparticles [45].

Yang et al. [48] reported that $(Mn, Co)_3O_4$ spinel demonstrated excellent electrical conductivity, satisfactory thermal and structural stability, as well as good thermal expansion match to ferritic stainless steel interconnects, and their results showed that $(Mn, Co)_3O_4$ spinel coating could act as a mass transport barrier to inhibit scale growth on the stainless steel and to prevent Cr outward migration through the coating. In this study, we combine the thermal stability and high electrical conductivity of Co_2MnO_4 spinels and highly catalytic active Pd nanoparticles to develop Co_2MnO_4 and PdO co-impregnated LCCM cathode for the IT-SOFCs. It is expected that Pd nanoparticles would significantly enhance the electrochemical performance of LCCM cathodes while the co-impregnation of Co_2MnO_4 spinel nanoparticles would significantly improve the microstructure stability of the infiltrated Pd nanoparticles without detrimental effect on the electrical conductivity of Pd nanoparticles.

2. Experimental

2.1. Synthesis and preparation of powders, YSZ electrolyte and LCCM electrodes

$La_{0.7}Ca_{0.3}Cr_{0.5}Mn_{0.5}O_{3-\delta}$ (LCCM) powders were prepared by glycine nitrate combustion process (GNP). Stoichiometry amount of hydrated nitrate salts of lanthanum, calcium, chromium and manganese (all from Sigma–Aldrich) were weighed and dissolved in distilled water with the addition of glycine ($C_2H_5NO_2$). The resultant solution was boiled until the liquid phase evaporated and the LCCM precursor formed in the form of ash. The obtained ashes were baked at 1000 °C for 6 h in air to form LCCM powder. Stoichiometric amounts of palladium nitrate ($Pd(NO_3)_2$, 10 wt% of $Pd(NO_3)_2$ in 10 wt% nitric acid solution), cobalt nitrate ($Co(NO_3)_2{\cdot}6H_2O$), and manganese nitrate ($Mn(NO_3)_2{\cdot}4H_2O$) (all from Sigma–Aldrich) were dissolved in distilled water. The atomic ratio of Co to Mn in the solution was 2. Then a stoichiometric amount of glycine (NH_2–CH_2–COOH, Alfa-Aesar) was added to the solution and the solution was boiled to evaporate excess water. The resulting viscous liquid was ignited and combusted to form black ash. The ash was baked between 400 °C and 900 °C in air for 5 h to obtain as-synthesized mixed PdO/Co_2MnO_4 powders. PdO, Co_2MnO_4 (CM), 10 wt% PdO/90 wt% Co_2MnO_4 (denoted as CM10Pd), 50 wt% PdO/50 wt% Co_2MnO_4 (denoted as CM50Pd) and 90 wt% PdO/10 wt% Co_2MnO_4 (denoted as CM90Pd) powders were synthesized to study the effect of Co_2MnO_4 spinels on the thermal and microstructure stability of PdO nanoparticles.

YSZ electrolyte substrates were prepared by die pressing of 8 mol% Y_2O_3–ZrO_2 powders (YSZ, Tosoh, Japan), followed by sintering at 1500 °C for 4 h in air. LCCM powders were mixed with an ink Vehicle (VEH, Fuel Cell Materials, Inc., USA) to form the LCCM paste. The electrode paste was painted to the YSZ electrolyte disk and sintered at 1200 °C in air for 2 h to produce LCCM cathode. The thickness and the surface area of the cathode after sintering were ~40 μm and 0.5 cm^2, respectively. Platinum paste (Pt ink 6082, Metalor, Singapore) was painted onto the other side of the electrolyte disk to make the counter and reference electrodes. The counter electrode was symmetrically positioned opposite of the cathode and the reference electrode was painted as a ring at the edge of the electrolyte substrates. The gap between the counter and ring reference electrode was 4 mm.

Infiltration solutions were prepared using $Pd(NO_3)_2$, $Co(NO_3)_2{\cdot}6H_2O$, and $Mn(NO_3)_2{\cdot}4H_2O$ with compositions of PdO, CM90Pd, CM50Pd, CM10Pd, CM. Solution infiltration of the LCCM electrode coating was carried out by placing a drop of the solution on top of the coating and let the solution penetrated into the porous cathode coating in air by the capillary force. Then the infiltrated samples were baked at 800 °C in air for 30 min. The mass of the sample before and after the infiltration treatment was measured to estimate the impregnated oxide loading. The loading was increased by repeating the solution infiltration processes.

2.2. Characterization and electrochemical activity measurements

Phases of the as-synthesized powders were determined by X-ray diffraction (XRD, Shimadzu, XRD-6000, X-Ray Diffractometer) using $CuK_{\alpha 1}$ radiation (λ = 1.54060 Å) at room temperature. X-ray scans were run over a 2θ spectrum of 20°–80° at a scan rate of 4° min^{-1}. Thermal behavior of the as-synthesized powders was analyzed on a 2950 thermal analyzer (TA Instruments Inc., New Castle, DE) with a heating rate of 10 °C min^{-1} under air flow of 50 mL min^{-1}. Scanning electron microscopy (SEM, JEOL 6360, Japan) was employed to investigate the morphology of as-synthesized powders.

The electrochemical activity for the O_2 reduction reaction on the LCCM cathode with and without infiltration was characterized by the electrochemical impedance spectroscopy (EIS) and polarization techniques. The EIS was measured at open circuit potential (OCP), using a Solartron 1260 frequency response analyzer in conjunction with a 1287 electrochemical interface at a frequency range of 100 kHz to 0.1 Hz with the signal amplitude of 10 mV. The sample was heated up to 900 °C, and the impedance measurements were conducted at different temperatures during cooling. The electrode interfacial (polarization) resistance (R_E) was determined by the difference between high and low frequency intercepts in the impedance axis, and the electrode ohmic resistance (R_Ω) was measured from the high frequency intercept. A cathodic current of 200 mA cm^{-2} was applied at 800 °C for up to 50 h to study the stability behavior of the cathodes. Overpotential (η) was obtained from $E_{cathode}$ and R_Ω by the following equation:

$$\eta = E_{cathode} - jR_\Omega \quad (1)$$

where j is the current density and $E_{cathode}$ is the cathode potential. The microstructure of LCCM cathode with and without impregnation before and after polarization study was inspected by a field emission scanning electron microscopy (FESEM, JEOL 6340F, Japan).

3. Results and discussion

3.1. Thermal behavior and microstructure of as-synthesized powders

Fig. 1 shows the XRD patterns of the prepared CM, LCCM and CM-impregnated LCCM cathode (baked at 900 °C for 50 h), PdO, CM90Pd, CM50Pd and CM10Pd powders baked at different temperatures for 5 h. As evidenced from Fig. 1a, the XRD pattern of the Co_2MnO_4 precursor heat-treated at 400 °C is consistent with the reported data of Co_2MnO_4 (JCPDS Card No. 84-0482), which indicates that the Co_2MnO_4 spinel structure started to form at 400 °C. As the heat treatment temperature increases, the intensity of the XRD peaks increases, indicating the increased crystallization of the spinel phase. There is no second phase detected in the XRD pattern of the Co_2MnO_4 powders heated at 900 °C for 5 h, indicating that

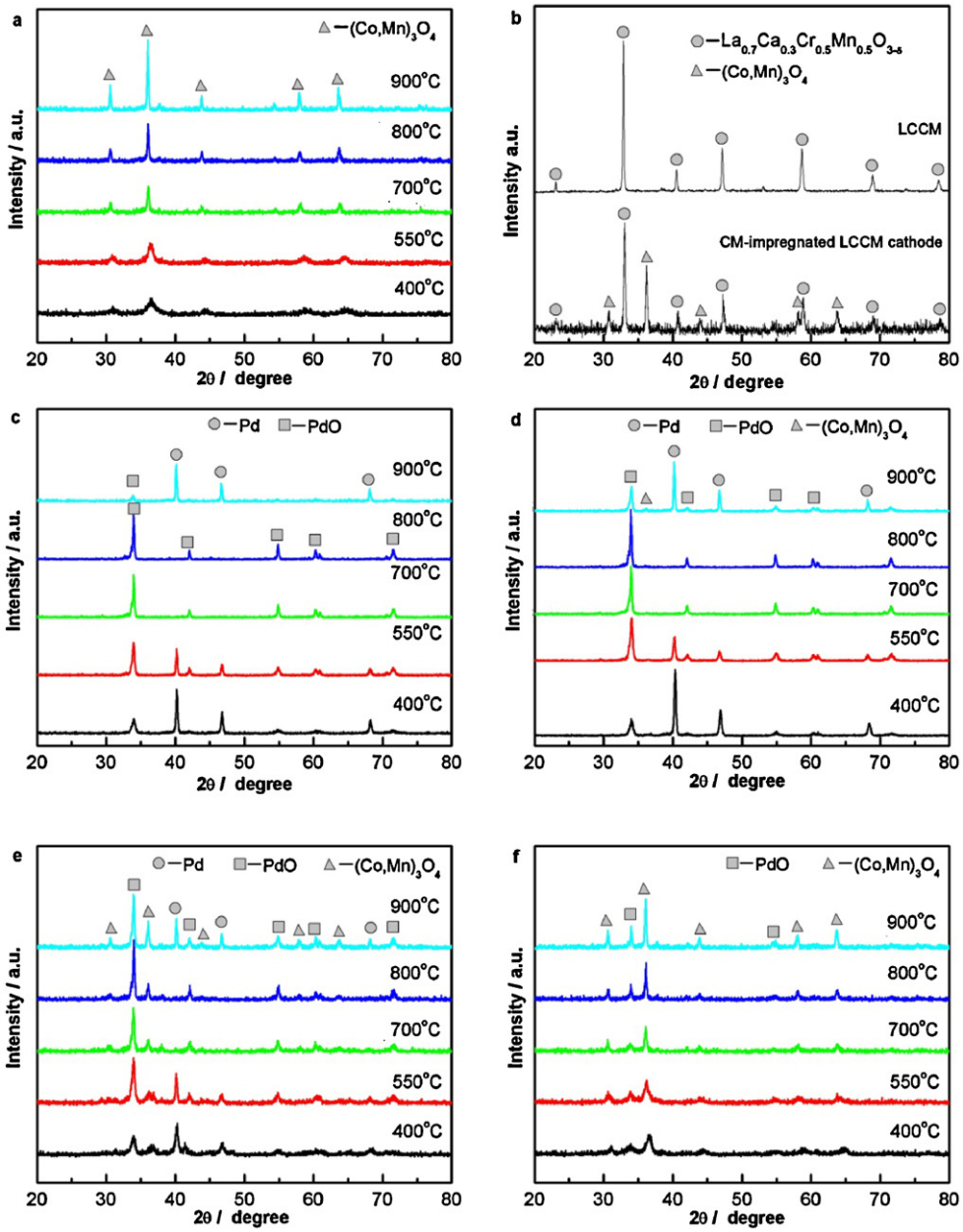

Fig. 1. XRD patterns of (a) Co_2MnO_4 (CM), (b) LCCM baked at 1000 °C for 6 h and CM impregnated LCCM, (c) PdO, (d) CM90Pd, (e) CM50Pd and (f) CM10Pd powders calcined at different temperatures for 5 h in air.

Co_2MnO_4 spinel oxide is structurally and thermally stable under high temperature up to 900 °C. XRD pattern of the synthesized LCCM matched well with the corresponding reference data of the LCCM powder (see Fig. 1b) [23,49], indicating the formation of the perovskite structure. The XRD pattern of the Co_2MnO_4-infiltrated LCCM (or CM-LCCM for short) cathode powders collected from the YSZ substrates after the heat-treatment at 900 °C for 50 h showed the formation of $(Co,Mn)_3O_4$ spinel-type oxide in the porous LCCM structure. No third phase except for the CM and LCCM was found in the XRD patterns, indicating chemical compatibility of $(Co,Mn)_3O_4$ spinel and LCCM phases under SOFC operating temperatures of 900 °C.

Fig. 1c–f shows the XRD patterns of the Co_2MnO_4–PdO (or CM–PdO) series powders calcined at different temperatures for 5 h in air. The phase of palladium changes with the heat treatment temperatures. At temperatures below 800 °C palladium exists as PdO (Fig. 1c). Metallic Pd was detected when the heat treatment temperature was 900 °C, indicating that the PdO oxides decompose at temperatures over 800 °C. The observed phase transformation temperature of 800–900 °C for PdO–Pd is consistent with that reported by Liang et al. [46]. Similar phase transformation was also observed on the mixed CM–PdO powders (Fig. 1d–f). However, different from pure Pd powders, the presence of Co_2MnO_4 affects the phase transformation between PdO and Pd. This is clearly indicated by the presence of PdO in the CM–PdO powders after the heat treatment at 900 °C and the intensity of the XRD peak of PdO increases with the increase of the Co_2MnO_4 in the mixture (Fig. 1d and e). In the case of CM–PdO with 90% Co_2MnO_4 and 10%PdO, no XRD peaks associated with metallic Pd were detected (Fig. 1f). This shows the increased stability of PdO phase at high temperatures, probably due to the presence of Co_2MnO_4 spinel. Furthermore, no other phase except for the Pd–PdO and Co_2MnO_4 was found in the XRD patterns, indicating the chemical compatibility of the Pd–PdO and spinel phases at temperatures up to 900 °C.

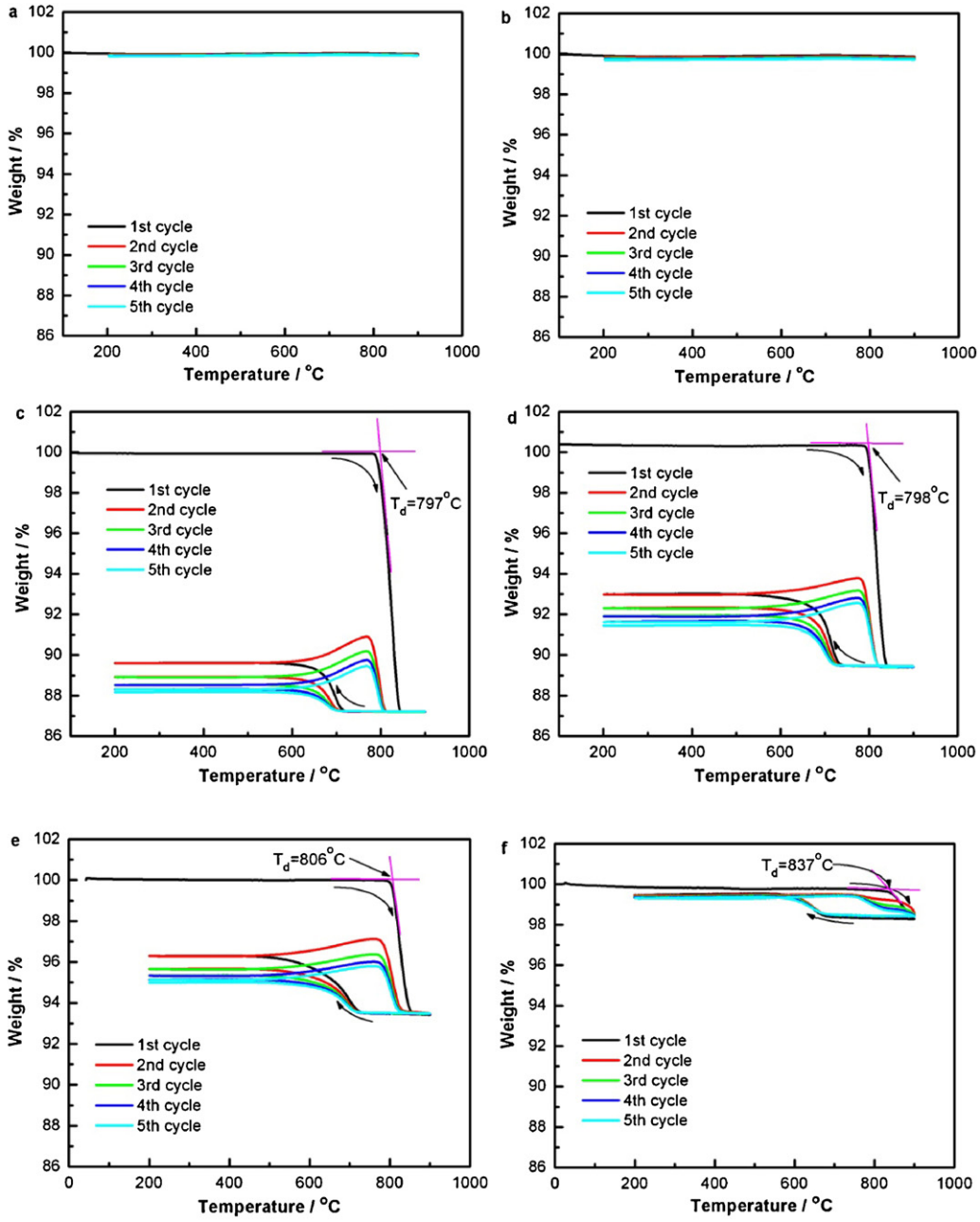

Fig. 2. TGA curves for (a) LCCM, (b) Co_2MnO_4 (CM), (c) PdO, (d) CM90Pd, (e) CM50Pd and (f) CM10Pd powders.

Before studying the electrochemical activity and stability of PdO and PdO–Co_2MnO_4 co-infiltrated LCCM cathode, the effect of spinel Co_2MnO_4 on the microstructure and thermal stability of PdO powders was investigated. Fig. 2 is the TGA results for LCCM, Co_2MnO_4, PdO, CM90Pd, CM50Pd and CM10Pd powders. There is no visible weight loss in both LCCM and Co_2MnO_4 powders (Fig. 2a and b), indicating the thermal stability of the LCCM and CM powders in the temperature range of 200–900 °C. The sudden weight loss observed in Fig. 2(c–f) is due to the decomposition of PdO to Pd. As shown in Fig. 2c, the decomposition temperature (T_d) of pure PdO is 797 °C that is almost identical to the results reported in reference [50]. Evidently, the phase transformation of Pd–PdO is not reversible. The weight percentage of the specimen is 87.2% after decomposed at 797 °C and the weight loss of 12.8% is due to the decomposition of PdO to Pd. However, during the reverse cycle the weight percentage of the specimen increased to 89.6%, an increase of ~2.4%. This corresponds to a convention rate of only 18.8% of metallic Pd to PdO (Fig. 2c). The low conversion rate indicates that majority of metallic Pd is not oxidized during the reverse cycle and the most likely reason is due to the significant agglomeration of palladium [46]. Increasing the cycling times did not improve the conversion rate (Fig. 2c).

As evidenced from Fig. 2d–f, the thermal behavior of the Co_2MnO_4–PdO mixed powders is very different. The decomposition temperature of PdO in CM90Pd, CM50Pd and CM10Pd powders is 798, 806 and 837 °C, respectively, and increases with the increased spinel oxides in the mixture. The conversion rate also increases significantly with the addition of Co_2MnO_4 spinel. In the case of CM50Pd specimen, the weight percentage of the specimen is 93.5% after decomposed at 806 °C and the weight loss of 6.5% is due to the decomposition of PdO to Pd. After the 1st reverse cycle the weight percentage of the specimen increased to 96.5%, an increase

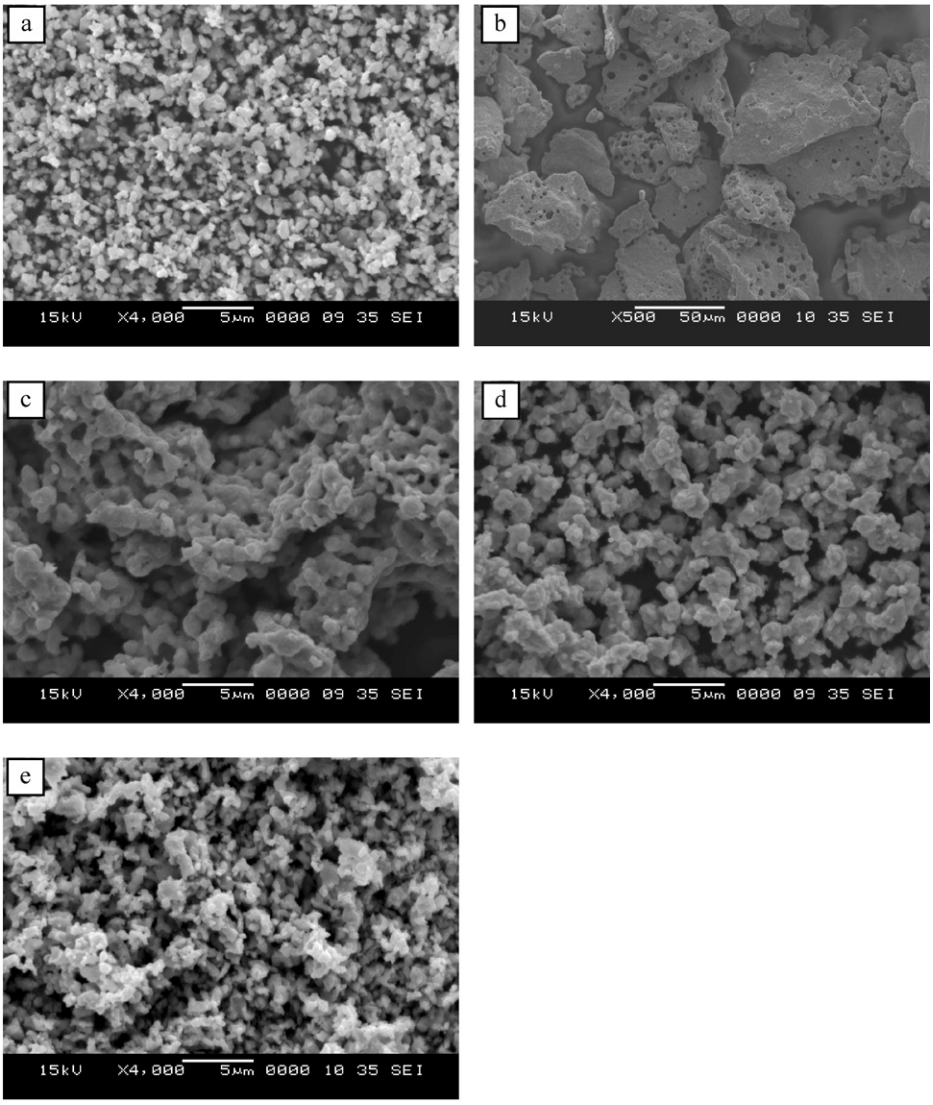

Fig. 3. SEM micrographs of the (a) Co_2MnO_4, (b) PdO, (c) CM90Pd, (d) CM50Pd and (e) CM10Pd powders calcined at 900 °C for 5 h in air.

of ~3.0%. This corresponds to a convention rate of 46% of metallic Pd to PdO (Fig. 2e). For the specimen of CM10Pd, the conversion rate is almost 100% (Fig. 2f). The significantly increased conversion rate shows that the presence of Co_2MnO_4 spinel inhibits the agglomeration of palladium.

The microstructure of the as-prepared Co_2MnO_4, PdO, CM90Pd, CM50Pd and CM10Pd powders after calcined at 900 °C for 5 h in air were examined by SEM and the results are shown in Fig. 3. The as-synthesized Co_2MnO_4 spinel powders consist of well-dispersed fine particles and the particle size is in the range of 0.7 ± 0.32 μm (Fig. 3a). After sintering at 900 °C for 5 h Pd particles sintered significantly, resulting in the formation of large agglomerates with size as large as 58 ± 30 μm (Fig. 3b). The significant agglomeration of palladium phase explains the significant thermal irreversibility as shown by the TGA analysis (Fig. 2c) as only the surface layer of the Pd agglomerates would be reactive with oxygen and oxidized during the reverse cycle. In contrast, the mixed CM–PdO particles demonstrated a significantly higher resistance to sintering. Instead of the formation of large particles, there is a formation of porous networks of Pd phase with Co_2MnO_4 particles (Fig. 3c). As the Co_2MnO_4 spinel in the Co_2MnO_4–PdO increases, there is clear formation of both PdO and Co_2MnO_4 particles and the particle size decreases with the Co_2MnO_4 contents (Fig. 3d and e). The presence of spinel oxides offers a significant resistance to the sintering of palladium phase. The SEM results are in a good agreement with the thermal behavior of the PdO and Co_2MnO_4–PdO mixed powders.

3.2. Effect of infiltration on the O_2 reduction reaction on LCCM cathode

Fig. 4 shows the impedance responses of LCCM with and without the Co_2MnO_4, PdO and CM/PdO impregnation, measured at 800 °C in air. In order to compare the polarization resistances, the ohmic resistances of different samples were adjusted to similar values. The impedance responses for the O_2 reduction reaction on pure LCCM cathode are characterized by a large impedance arc and the interfacial (polarization) resistance, R_E, is 3.59 Ω cm^2 (Fig. 4a). As shown in Fig. 4a, with the impregnation of 0.54, 0.9 and 1.4 mg cm^{-2} CM, R_E is reduced to 2.25, 1.65 and 0.5 Ω cm^2, respectively. The R_E for the reaction on 1.4 mg cm^{-2} CM-infiltrated LCCM is ~7 times smaller than that on the pure LCCM cathode.

Infiltration of palladium also shows the significant reduction in R_E for the reaction on LCCM cathodes. With the infiltration of 0.14, 0.28, 0.36, 0.51 and 0.64 mg cm^{-2} PdO, R_E is reduced to 1.44, 0.86, 0.33, 0.23 and 0.13 Ω cm^2, respectively (see Fig. 4b). The R_E for the O_2 reduction reactions on the 0.64 mg cm^{-2} PdO-impregnated

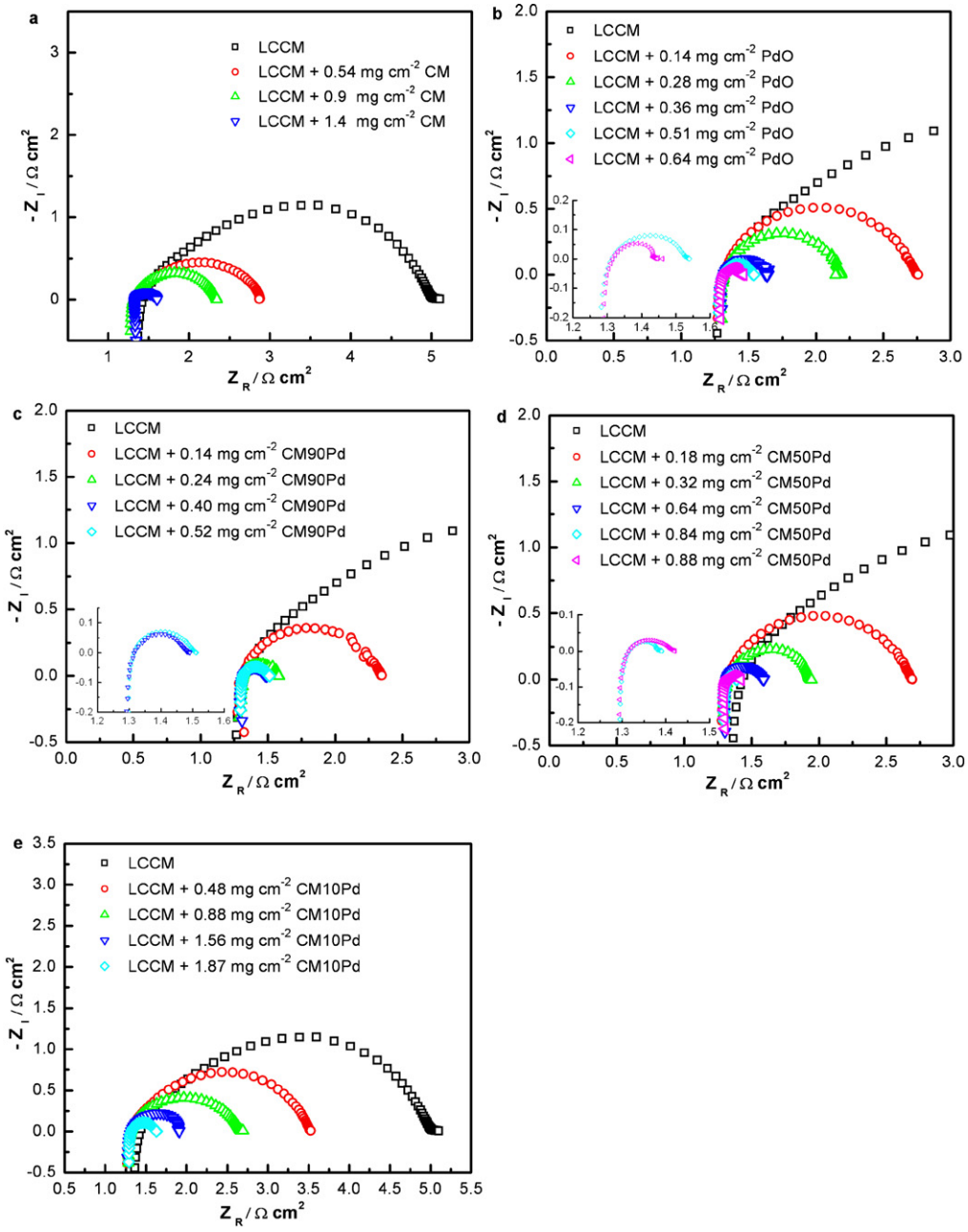

Fig. 4. Impedance responses of LCCM electrodes infiltrated with (a) Co_2MnO_4 (CM), (b) PdO, (c) CM90Pd, (d) CM50Pd and (e) CM10Pd, measured under open circuit potential at 800 °C in air.

LCCM cathode is ~28 times smaller than that for the O_2 reduction reactions on the pure LCCM and is also ~4 times smaller than that on the 1.4 mg cm^{-2} CM-infiltrated LCCM cathode. The substantial decrease of R_E for the O_2 reduction reactions on the PdO-infiltrated LCCM cathode is clearly related to the high electrocatalytic activity of the infiltrated PdO nanoparticles. The results also indicate that the electrocatalytic activity of PdO for the O_2 reduction reaction is higher than that of Co_2MnO_4 spinel phase. The significant performance enhancement with the impregnation of PdO nanoparticles has also been observed on $La_{0.8}Sr_{0.2}MnO_3$ cathode [34], $La_{0.8}Sr_{0.2}Co_{0.5}Fe_{0.5}O_3$ cathode [40], Pd + YSZ cathode [44]. The R_E value of ~0.13 Ω cm^2 for the O_2 reduction reaction on PdO-infiltrated LCCM at 800 °C is comparable to ~0.4 Ω cm^2 at 800 °C reported on GDC-impregnated LCCM cathode [28]. It has also been found that with the impregnation of 0.14, 0.28, 0.36, 0.51 and 0.64 mg cm^{-2} PdO, R_E at 700 °C is reduced from 35 Ω cm^2 to 14.6, 9.6, 8.7, 5.6 and 31.9 Ω cm^2, respectively. It is evidenced that further increase in the PdO loading higher than 0.51 mg cm^{-2} results in a degradation in the electrochemical activity of the electrodes especially at intermediate operating temperature. The deterioration of the electrochemical activity with high Pd loading was also observed for the H_2 oxidation reaction on Pd-infiltrated Ni/GDC cermet anodes [51].

With the impregnation of 0.14, 0.24, 0.40 and 0.52 mg cm^{-2} CM90Pd, R_E for the oxygen reduction reaction at 800 °C is 1.03, 0.27, 0.17 and 0.20 Ω cm^2, respectively (Fig. 4c). The R_E value of the 0.4 mg cm^{-2} CM90Pd-impregnated LCCM cathode is lower than that of 0.36 mg cm^{-2} PdO–impregnated LCCM cathode (0.17 Ω cm^2 vs. 0.33 Ω cm^2), although they contain same amount of PdO. The higher electrocatalytic activity of the former indicates that the presence of Co_2MnO_4 spinel phase can inhibit the agglomeration of PdO nanoparticles.

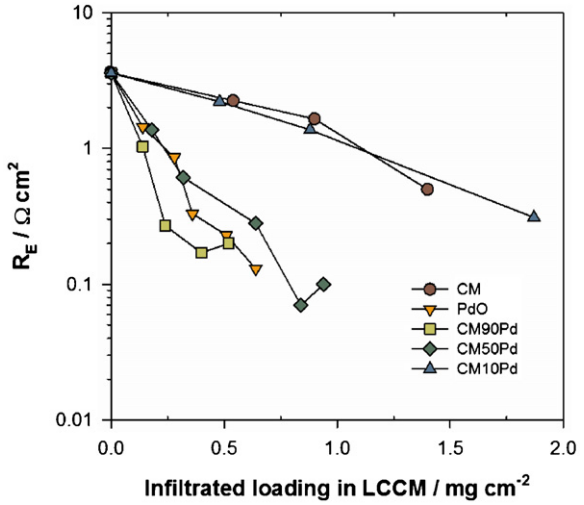

Fig. 5. Plots of electrode polarization resistance (R_E) for the O_2 reduction on LCCM cathodes as a function of infiltrated oxide loading.

As shown in Fig. 4d, the R_E of the LCCM cathode infiltrated with 0.18, 0.32, 0.64, 0.84 and 0.88 mg cm^{-2} CM50Pd is reduced from 3.59 Ω cm^2 to 1.37, 0.61, 0.28, 0.07 and 0.10 Ω cm^2, respectively. The R_E value of ~0.07 Ω cm^2 for the O_2 reduction reaction on CM50Pd-infiltrated LCCM at 800 °C is significantly lower than ~0.13 Ω cm^2 on PdO-infiltrated LCCM cathode and comparable to ~0.05 Ω cm^2 reported on Pd + YSZ cathode [44]. It is evidenced that the higher electrocatalytic activity of the CM50Pd-infiltrated LCCM cathode is due to a better separation of PdO-nanoparticles by co-infiltration of Co_2MnO_4 spinels.

The interfacial resistance of 0.48, 0.88 and 1.87 mg cm^{-2} CM10Pd-infiltrated LCCM cathode is 2.21, 1.37 and 0.31 Ω cm^2, respectively (Fig. 4e). Compared with the LCCM cathode with same CM loading, the R_E value for the O_2 reduction reaction on the CM10Pd-impregnated LCCM at 800 °C is slightly lower (~0.31 Ω cm^2 vs. ~0.5 Ω cm^2), probably improved by the small impregnated PdO nanoparticles.

The effect of the infiltrated PdO and CM–PdO loadings on the electrode polarization resistance is summarized in Fig. 5. The best result was obtained on infiltrated PdO and co-infiltration with PdO and Co_2MnO_4 spinels with 90/10 and 50/50 weight ratio (CM90Pd and CM50Pd). In the case of co-infiltrated PdO and Co_2MnO_4 spinels with 10/90 ratio, the electrocatalytic activity of LCCM is similar to that of Co_2MnO_4-infiltrated LCCM, significantly lower than that of infiltrated LCCM with PdO, CM90Pd and CM50Pd. The results show that excess Co_2MnO_4 spinels will reduce the electrocatalytic activity of the infiltrated phase as Co_2MnO_4 spinels are not as active electrochemically as that of PdO phase.

3.3. Electrochemical activity stability of impregnated LCCM cathode

Fig. 6 shows the impedance responses at open circuit potential and polarization curves of LCCM cathode with and without PdO- and CM–PdO-infiltration under a cathodic current density of 200 mA cm^{-2} for 50 h at 800 °C in air. The size of the impedance arcs for the O_2 reduction reaction on pristine LCCM cathode decreases with the cathodic current passage. After current passage for 60 min, R_E was reduced from an initial value of 3.59 Ω cm^2 to 1.96 Ω cm^2 and reached a stable value of 1.08 Ω cm^2 after polarized for 50 h (Fig. 6a). The initial polarization potential of the LCCM electrodes behaved similarly to the impedance behavior. As evidenced from Fig. 6b, the initial electrode potential, $E_{cathode}$ was very high, 1.15 V at 200 mA cm^{-2} before current passage. With a cathodic current passage, the cathode potential decreased very rapidly. After cathodic current treatment for 30 min, the $E_{cathode}$ was reduced from 1.15 V to 0.64 V. However, the change in $E_{cathode}$ with further current passage time is very small. The electrode ohmic resistance, R_Ω changed slightly changed from 1.39 Ω cm^2 to 1.52 Ω cm^2 after current passage for 50 h and is more or less stable. This indicates that the reduction in $E_{cathode}$ is mainly due to the overpotentials, η which is reduced from 865 mV to 135 mV. Such impedance and polarization behavior with cathodic current passage are identical to the well-known activation processes for the oxygen reduction on the LSM electrodes [52–55].

The initial impedance responses of LCCM cathode with 0.33 mg cm^{-2} PdO loading are very similar to that of the pure LCCM cathode (Fig. 6c). The impedance arc decreased with the cathodic current passage. After the current passage for 60 min, R_E of 0.33 mg cm^{-2} PdO-infiltrated LCCM cathode reduced from 0.66 Ω cm^2 to 0.40 Ω cm^2, which is significantly lower than 1.96 Ω cm^2 of pure LCCM cathode under identical cathodic current passage treatment. The overall $E_{cathode}$ decreases with the polarization time, similar to that of pure LCCM. However, the initial polarization potential of the PdO-infiltrated LCCM cathode behaved differently to that of the pure LCCM cathode. With a cathodic current passage, the cathode potential increased very rapidly initially, followed by a region where the increase in $E_{cathode}$ was much smaller (see the inset in Fig. 6d). The increase in $E_{cathode}$ is about 90–150 mV. The exact reason for such initial polarization potential behavior is not clear at this stage. The value of R_Ω was slightly increased from 0.60 Ω cm^2 to 0.68 Ω cm^2, which imply that the variation in $E_{cathode}$ was mainly due to the variation in overpotentials, η. The η of PdO-infiltrated LCCM cathode gradually decreased and finally stabilized at ~45 mV, significantly lower 135 mV of pristine LCCM cathode. The result demonstrates a much more improved electrochemical performance for the O_2 reduction reactions than the pure LCCM cathode.

In contrast to that of the pristine LCCM and PdO-infiltrated LCCM cathodes, the initial impedance of LCCM cathode with 1.4 mg cm^{-2} CM loading increased with the cathodic polarization treatment (Fig. 6e). After the current passage for 50 h, R_E was increased from 0.25 Ω cm^2 to 0.54 Ω cm^2. Similar to the impedance behavior, the $E_{cathode}$ and η of the CM-infiltrated LCCM cathode show an increase with the cathodic current passage and become stable after being polarized for ~3 h. Also different to that of LCCM cathode, R_Ω increases with the cathodic polarization time and it increased from 0.5 Ω cm^2 to 0.88 Ω cm^2 after cathodic polarization for 50 h. Nevertheless, the R_E and η for the reaction on the CM-infiltrated LCCM cathode are lower than that on the pure LCCM cathode tested under the same conditions. This indicates that the incorporation of the nanosized Co_2MnO_4 nanoparticles enhances the electrocatalytic activity of the LCCM cathode.

The initial impedance and polarization behavior of LCCM cathode infiltrated with 0.72 mg cm^{-2} CM50Pd are similar to that of CM-infiltrated LCCM cathodes, but the magnitude of the increase in $E_{cathode}$ and R_Ω is much smaller (Fig. 6g and h). After the current passage for 50 h, R_E was 0.25 Ω cm^2, significantly lower than that of pristine LCCM cathode. The significant differences in the electrode behavior of the LCCM and CM50Pd-infiltrated LCCM indicate that the activation effect of cathodic polarization is no longer effective for the O_2 reduction reaction on the CM50Pd-infiltrated LCCM cathode. The $E_{cathode}$ and η of the CM50Pd-infiltrated LCCM cathode also show an increase with the cathodic current passage and become stable after being polarized for ~6 h. The η of the CM50Pd-impregnated LCCM cathode after being polarized at 200 mA cm^{-2} for ~6 h is 65 mV. Despite the increase in R_E and η, the stabilized R_E and η for the reaction on the CM50Pd-impregnated LCCM cathode are only ~ 19 and 42% of those on the pristine LCCM cathode tested under the same conditions. This

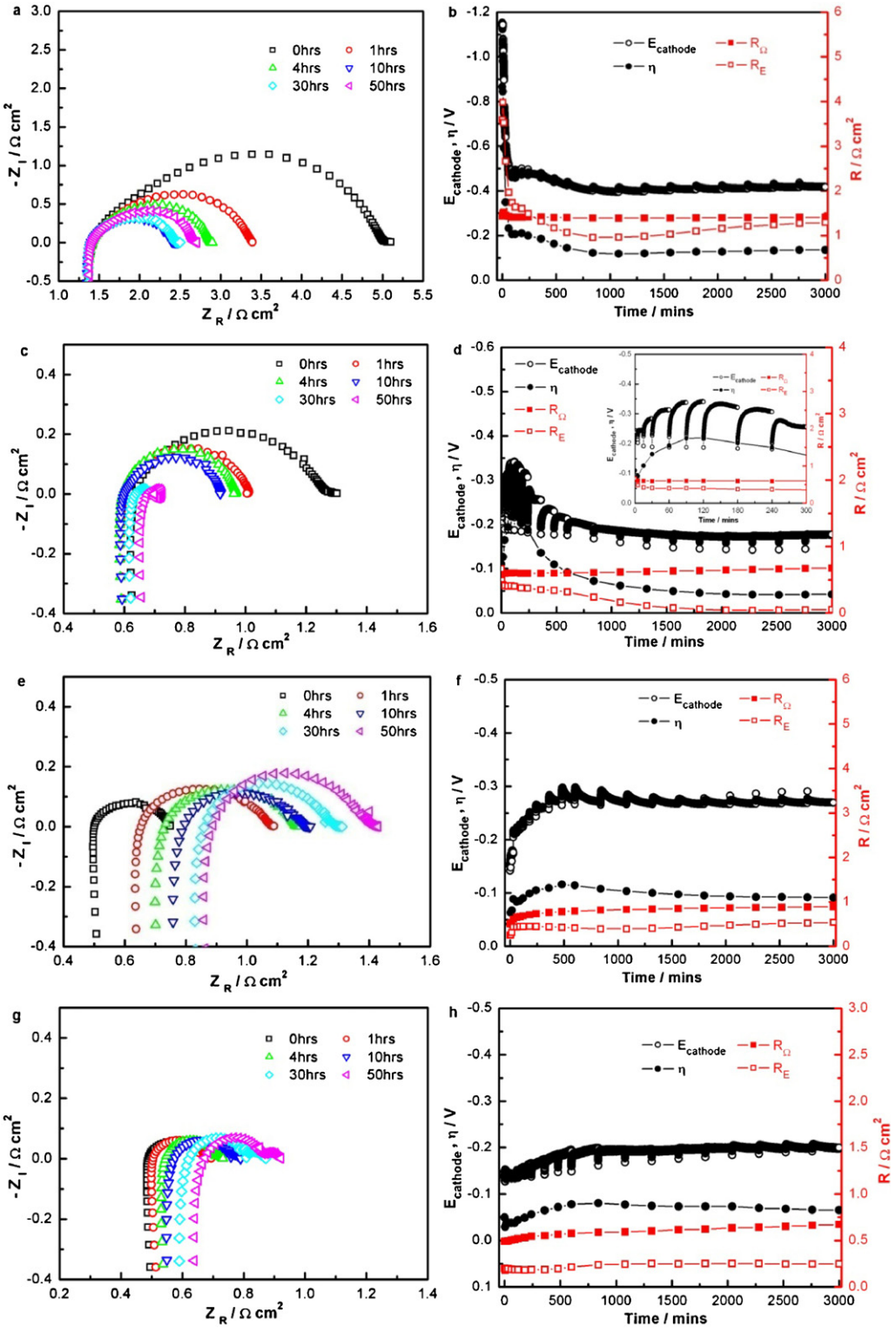

Fig. 6. Electrochemical impedance spectra and polarization performance as a function of polarization time for the O_2 reduction reaction on (a and b) pure LCCM electrode, (c and d) 0.33 mg cm^{-2} PdO-infiltrated LCCM, (e and f) 1.4 mg cm^{-2} CM-infiltrated LCCM and (g and h) 0.72 mg cm^{-2} CM50Pd-infiltrated LCCM. The impedance curves were measured at 800 °C and open circuit before and after polarization under 200 mA cm^{-2} for different period.

demonstrates that the incorporation of the nanosized CM and PdO mixed particles not only increases the electrocatalytic activity but also enhances the life performance of the LCCM cathode. The η value of CM50Pd-infiltrated LCCM cathode was stabilized at ~65 mV after cathodic polarization for 50 h, very close to the value of 45 mV, measured on PdO-infiltrated LCCM cathode. This indicates that the co-infiltrated Co_2MnO_4–PdO is equally effective to promote the electrocatalytic activity of LCCM electrodes but with

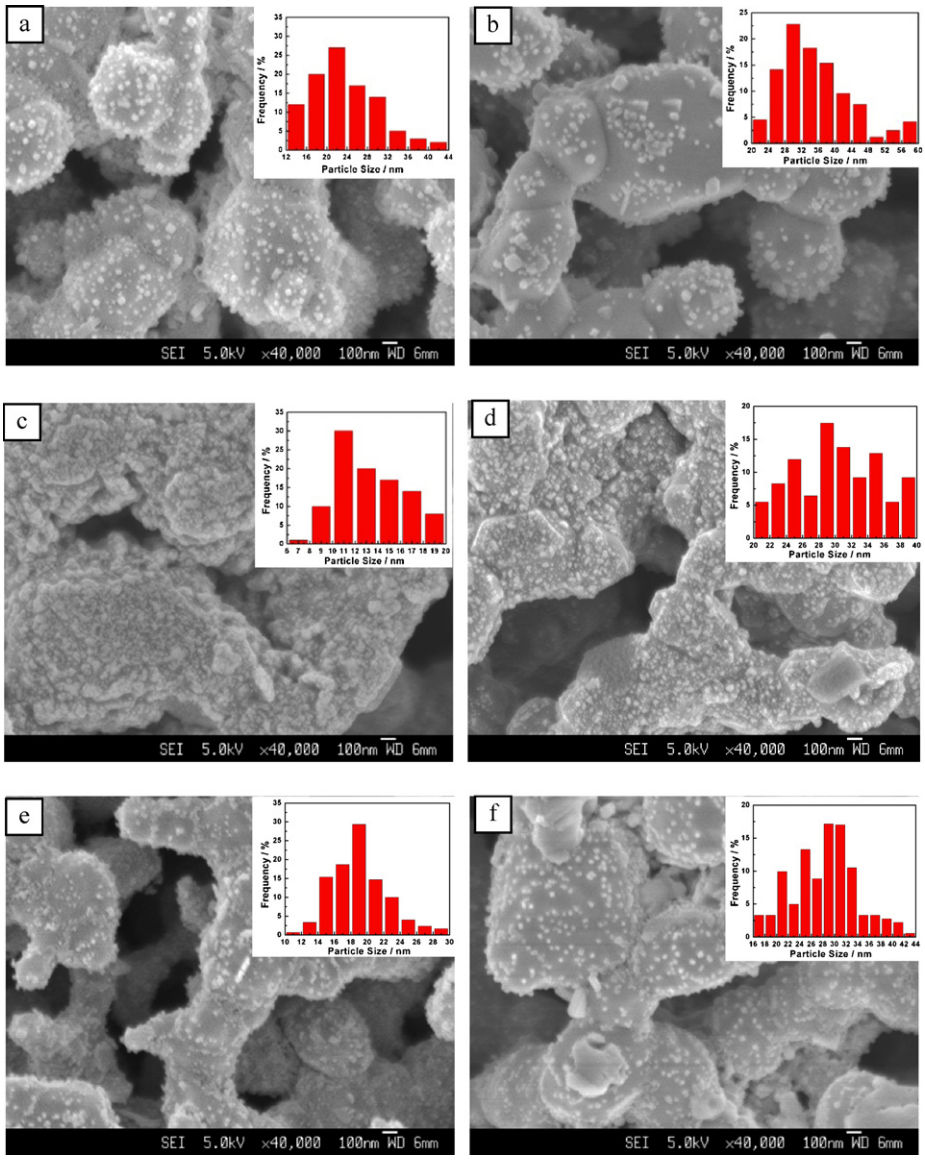

Fig. 7. FESEM micrographs of LCCM cathode with (a and b) 0.33 mg cm^{-2} PdO-infiltrated LCCM, (c and d) 1.4 mg cm^{-2} CM-infiltrated LCCM and (e and f) 0.72 mg cm^{-2} CM50Pd-infiltrated LCCM. The images a, c and e are before and b, d and f are after the polarization treatment.

significantly enhanced thermal stability as shown in Fig. 2 as well as microstructure stability as will be discussed in the following sections.

3.4. Microstructure of the infiltrated LCCM cathode

Fig. 7 shows the FESEM micrographs of the surface of PdO, Co_2MnO_4 and Co_2MnO_4–PdO infiltrated LCCM electrodes before and after cathodic galvanostatic treatment at 200 mA cm^{-2} and 800 °C for 50 h. The histogram of the size distribution of infiltrated nanoparticles is also shown in the figure. As evidenced from Fig. 7a, the initial size of fine PdO particles on the LCCM surface is ~22 nm with symmetric distribution. After cathodic current treatment there is significant agglomeration of PdO nanoparticles with substantial reduced fine particles (Fig. 7b). The average size of PdO nanoaprticles is ~35 nm but there are large numbers of PdO particles in the range of 50–60 nm. The agglomeration of finely distributed PdO nanoparticles is clearly due to the cathodic polarization treatment at 800 °C. In the case of infiltrated CM, the initial spinel particles were in the range of ~11 nm and increased to ~30 nm after the cathodic current treatment (Fig. 7c and d).

In the case of CM50Pd co-infiltrated LCCM electrodes, the initial particle size was ~19 nm in average and grew to ~29 nm after cathodic current passage at 200 mA cm^{-2} and 800 °C for 50 h (Fig. 7e and f). The change of the co-infiltrated Co_2MnO_4–PdO nanoparticles is relatively small. Different to that of pure PdO nanoparticles, there is no visible agglomeration of the co-infiltrated CM50Pd nanoparticles and the distribution of the Co_2MnO_4–PdO nanoparticles is close to that before the polarization (Fig. 7f). The SEM results clearly show that co-infiltration of Co_2MnO_4 spinel significantly stabilizes the PdO nanoparticles. This explains the better electrochemical performance of the Co_2MnO_4 and PdO co-infiltrated LCCM cathode, as compared to that of the PdO- and Co_2MnO_4-infiltrated LCCM cathode (see Figs. 4 and 5). The improved microstructure stability is particular important for the long-term stability of nanostructured electrodes operated under IT-SOFCs conditions.

4. Conclusions

The effect of co-infiltration of Co_2MnO_4 on the microstructure and thermal stability of PdO and electrochemical performance and

stability of the PdO-infiltrated $La_{0.7}Ca_{0.3}Cr_{0.5}Mn_{0.5}O_{3-\delta}$ cathodes for the O_2 reduction reaction were investigated and the following conclusions can be obtained:

1 Pd/PdO and Co_2MnO_4 powders are chemically compatible. The presence of Co_2MnO_4 spinel increases the decomposition temperature of PdO to metallic Pd and significantly improves the conversion rate of Pd to PdO during the thermal recycle. Adding Co_2MnO_4 to PdO significantly inhibits the agglomeration and grain growth of PdO/Pd nanoaprticles of the infiltrated LCCM cathodes due to the significantly inhibiting effect of spinel oxides on the agglomeration of Pd/PdO nanoparticles.
2 The infiltration of PdO, Co_2MnO_4 and Co_2MnO_4–PdO enhances the electrochemical performance of the LCCM cathodes for the oxygen reduction reaction. Co-infiltrated LCCM cathode with 50 wt% PdO and 50 wt% Co_2MnO_4 (CM50Pd) exhibits the significantly enhanced electrochemical activity and performance stability. The enhancement is evidently due to the stable Co_2MnO_4–PdO nanoparticles under IT-SOFCs operation conditions, as shown by the SEM results.

Acknowledgements

This work is supported by the academic research fund AcRF tier 2 (MOE2009-T2-2-024), Ministry of Education, Singapore and competitive research program (2009 NRF-CRP 001-032), National Research Foundation, Singapore, and ARC Linkage Project (LP110200281), Australia.

References

[1] E.V. Tsipis, V.V. Kharton, J. Solid State Electrochem. 12 (2008) 1367.
[2] C.W. Sun, R. Hui, J. Roller, J. Solid State Electrochem. 14 (2010) 1125.
[3] L. Jian, C.Y. Yuh, M. Farooque, Corros. Sci. 42 (2000) 1573.
[4] L. Zhang, S.P. Jiang, W. Wang, Y.J. Zhang, J. Power Sources 170 (2007) 55.
[5] L. Zhang, H.Q. He, W.R. Kwek, J. Ma, E.H. Tang, S.P. Jiang, J. Am. Ceram. Soc. 92 (2009) 302.
[6] C.H. Zhao, R.Z. Liu, S.R. Wang, T.L. Wen, Electrochem. Commun. 11 (2009) 842.
[7] X.Q. Huang, L. Pei, Z.G. Liu, Z. Lu, Y. Sui, Z.N. Qian, W.H. Su, J. Alloy. Compd. 345 (2002) 265.
[8] Y. Ji, J. Liu, T.M. He, L.G. Cong, J.X. Wang, W.H. Su, J. Alloy. Compd. 353 (2003) 257.
[9] D.G. Lamas, M.F. Bianchetti, M.D. Cabezas, N.E.W. de Reca, J. Alloy. Compd. 495 (2010) 548.
[10] B. Hua, J. Pu, J.F. Zhang, F.S. Lu, B. Chi, L. Jian, J. Electrochem. Soc. 156 (2009) B93.
[11] B. Hua, F. Lu, J. Zhang, Y. Kong, J. Pu, B. Chi, L. Jian, J. Electrochem. Soc. 156 (2009) B1261.
[12] L. Jian, P. Jian, J.H. Xiao, X.L. Qian, J. Power Sources 139 (2005) 182.
[13] S.P. Jiang, W. Wang, Solid State Ionics 176 (2005) 1351.
[14] S.P. Jiang, J. Mater. Sci. 43 (2008) 6799.
[15] S.P. Jiang, W. Wang, Solid State Ionics 176 (2005) 1185.
[16] N.P. Brandon, S. Skinner, B.C.H. Steele, Annu. Rev. Mater. Res. 33 (2003) 183.
[17] H. Yokokawa, Annu. Rev. Mater. Res. 33 (2003) 581.
[18] S.P. Jiang, J. Power Sources 124 (2003) 390.
[19] S. Carter, A. Selcuk, R.J. Chater, J. Kajda, J.A. Kilner, B.C.H. Steele, Solid State Ionics 53 (1992) 597.
[20] R.A. De Souza, J.A. Kilner, J.F. Walker, Mater. Lett. 43 (2000) 43.
[21] S.P. Jiang, J.P. Zhang, K. Foger, J. Eur. Ceram. Soc. 23 (2003) 1865.
[22] A. Chen, G. Bourne, K. Siebein, R. DeHoff, E. Wachsman, K. Jones, J. Am. Ceram. Soc. 91 (2008) 2670.
[23] S.W. Tao, J.T.S. Irvine, J. Electrochem. Soc. 151 (2004) A252.
[24] S.W. Tao, J.T.S. Irvine, Nature Mater. 2 (2003) 320.
[25] E.S. Raj, J.A. Kilner, J.T.S. Irvine, Solid State Ionics 177 (2006) 1747.
[26] L. Zhang, S.P. Jiang, C.S. Cheng, Y.J. Zhang, J. Electrochem. Soc. 154 (2007) B577.
[27] S.P. Jiang, L. Zhang, Y. Zhang, J. Mater. Chem. 17 (2007) 2627.
[28] L. Zhang, X.B. Chen, S.P. Jiang, H.Q. He, Y. Xiang, Solid State Ionics 180 (2009) 1076.
[29] S.P. Jiang, L. Liu, P.O.B. Khuong, W.B. Ping, H. Li, H. Pu, J. Power Sources 176 (2008) 82.
[30] K.P. Ong, P. Wu, L. Liu, S.P. Jiang, Appl. Phys. Lett. 90 (2007) 0441091.
[31] S.P. Jiang, Mater. Sci. Eng. A: Struct. Mater. Prop. Microstruct. Process. 418 (2006) 199.
[32] Z.Y. Jiang, C.R. Xia, F.L. Chen, Electrochim. Acta 55 (2010) 3595.
[33] J.M. Vohs, R.J. Gorte, Adv. Mater. 21 (2009) 943.
[34] F.L. Liang, J. Chen, S.P. Jiang, B. Chi, J. Pu, L. Jian, Electrochem. Solid State Lett. 11 (2008) B213.
[35] S.P. Jiang, W. Wang, J. Electrochem. Soc. 152 (2005) A1398.
[36] J. Chen, F.L. Liang, B. Chi, J. Pu, S.P. Jiang, L. Jian, J. Power Sources 194 (2009) 275.
[37] F. Zhao, L. Zhang, Z.Y. Jiang, C.R. Xia, F.L. Chen, J. Alloy. Compd. 487 (2009) 781.
[38] T.J. Armstrong, J.G. Rich, J. Electrochem. Soc. 153 (2006) A515.
[39] F.L. Liang, J. Chen, S.P. Jiang, B. Chi, J. Pu, L. Jian, Electrochem. Commun. 11 (2009) 1048.
[40] M. Sahibzada, S.J. Benson, R.A. Rudkin, J.A. Kilner, Solid State Ionics 113 (1998) 285.
[41] N. Ai, S.P. Jiang, Z. Lu, K.F. Chen, W.H. Su, J. Electrochem. Soc. 157 (2010) B1033.
[42] C. Lu, T.Z. Sholklapper, C.P. Jacobson, S.J. Visco, L.C. De Jonghe, J. Electrochem. Soc. 153 (2006) A1115.
[43] Z.Y. Jiang, L. Zhang, L.L. Cai, C.R. Xia, Electrochim. Acta 54 (2009) 3059.
[44] F.L. Liang, J. Chen, J.L. Cheng, S.P. Jiang, T.M. He, J. Pu, J. Li, Electrochem. Commun. 10 (2008) 42.
[45] N. Imanishi, R. Ohno, K. Murata, A. Hirano, Y. Takeda, O. Yamamoto, K. Yamahara, Fuel Cells 9 (2009) 215.
[46] F.L. Liang, J. Chen, S.P. Jiang, F.Z. Wang, B. Chi, J. Pu, L. Jian, Fuel Cells 9 (2009) 636.
[47] A. Babaei, L. Zhang, E.J. Liu, S.P. Jiang, J. Alloy. Compd. 509 (2011) 4781.
[48] Z.G. Yang, G.G. Xia, X.H. Li, J.W. Stevenson, Int. J. Hydrogen Energ. 32 (2007) 3648.
[49] A. Babaei, L. Zhang, S.L. Tan, S.P. Jiang, Solid State Ionics 181 (2010) 1221.
[50] H. Zhang, J. Gromek, M. Augustine, G. Fernando, R.S. Boorse, H.L. Marcus, Phys. B: Condens. Matter 344 (2004) 278.
[51] A. Babaei, S.P. Jiang, J. Li, J. Electrochem. Soc. 156 (2009) B1022.
[52] S.B. Adler, Chem. Rev. 104 (2004) 4791.
[53] S.P. Jiang, J.G. Love, Solid State Ionics 138 (2001) 183.
[54] S.P. Jiang, J.G. Love, J.P. Zhang, M. Hoang, Y. Ramprakash, A.E. Hughes, S.P.S. Badwal, Solid State Ionics 121 (1999) 1.
[55] W. Wang, S.P. Jiang, Solid State Ionics 177 (2006) 1361.